ACS NANO
Cite This: ACS Nano 2018, 12, 11860−11870
www.acsnano.org

ARTICLE

Single Molecular Layer of Silk Nanoribbon as Potential Basic Building Block of Silk Materials

Qianqian Niu,[†] Qingfa Peng,[†,§] Li Lu,[†] Suna Fan,[†] Huili Shao,[†] Huihui Zhang,[†] Rongliang Wu,*[,†] Benjamin S. Hsiao,*[,‡] and Yaopeng Zhang*[,†]

[†]State Key Laboratory for Modification of Chemical Fibers and Polymer Materials, International Joint Laboratory for Advanced Fiber and Low-Dimension Materials, College of Materials Science and Engineering, Donghua University, Shanghai, 201620, China
[‡]Department of Chemistry, Stony Brook University, Stony Brook, New York 11794-3400, United States

Supporting Information

ABSTRACT: In this study, nascent silk nanoribbons (SNRs) with an average thickness of 0.4 nm were extracted from natural silkworm silk by partially dissolving degummed silk (DS) in sodium hydroxide (NaOH)/urea solution at −12 °C. In this gentle treatment, the solvent could not destroy the nanofibrillar structure completely, but the chosen conditions would influence the dimensions of resulting SNRs. Molecular dynamics simulations of silk models indicated that the potential of mean force required to break hydrogen bonds between silk fibroin chains was 40% larger than that of van der Waals interactions between β-sheet layers, allowing the exfoliating treatment. It was found that the resulting SNRs contained a single β-sheet layer and amorphous silk fibroin molecules, which could be considered as the basic building block of DS consisting of hierarchical structures. The demonstrated technique for extracting ultrathin SNRs having the height of a single β-sheet layer may provide a useful pathway for creating stronger and tougher silk-based materials and/or adding functionality and durability in materials for various applications. The hierarchical structure model based on SNRs may afford more insight into the structure and property relationship of fabricating silk-based materials.

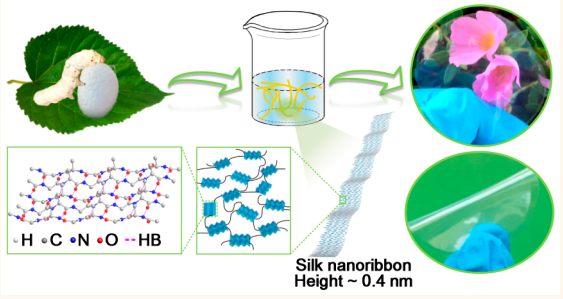

KEYWORDS: *NaOH/urea solution, low temperature, silk nanoribbons, single β-sheet layer, hierarchical structure*

Silkworm silks contain hierarchical structures of amorphous chains and stacked β-sheets.[1−4] The properties of silk-based materials are closely related to the structure of the unique spatial arrangement at either mesoscale or nanoscale.[5,6] It is well known that a small change of the structure in either scale can cause notable property change in the resulting product.[7,8] For example, it has been reported that mechanical properties of silk-based materials are directly associated with the hierarchical structures[9−11] such as molecular β-crystalline and fibrillar structures.[12−14] As the nanoscale fibrillar structure plays an important role in the performance of native silk,[12,15] it is usually a good choice that native silks, containing fundamental building blocks of silk, are employed to fabricate silk-based materials in order to retain the strengths of natural materials.[16]

Silk nanofibrils (SNFs) from *Bombyx mori* (*B. mori*) silkworm have been routinely used as the assembly element or reinforcing agent to prepare functional materials[17,18] or composite materials.[16,19,20] Both bottom-up and top-down approaches have been demonstrated to fabricate SNFs. The bottom-up method involves the use of silk fibroin solutions, in combination with ultrasonic,[21] shear,[22] and other external mechanical treatments,[23−26] to self-assemble proteins into SNFs, whereby the typical width of SNFs ranges from 3 to 70 nm and the thickness is over 1 nm.[21−23,27−31] In this approach, silk fibroin is first obtained by destroying hydrogen bonds between silk fibroin molecules through the dissolution of degummed silk (DS) by varying solvents, such as inorganic salt solutions (lithium bromide (LiBr) aqueous solution[25,32] and calcium chloride ($CaCl_2$)/ethanol/H_2O solution),[33] concentrated acids,[34] and ionic liquids.[35] As the fibrillar structure is destroyed during the silk dissolution step, the structure of regenerated silk nanofibers becomes different from native silk. As a result, the properties of materials produced by SNFs are often inferior to natural silk. Furthermore, achieving well-dispersed SNFs suspension remains to be a challenge.[18,36] On the other hand, the top-down method involves the incomplete dissolution of DS using weaker solvents, such as HCl/formic acid (FA),[37] FA-$CaCl_2$,[20,38] FA-LiBr,[36] and hexafluoroisopropanol (HFIP).[16−18] These solvents possess only marginal

Received: May 24, 2018
Accepted: November 5, 2018
Published: November 8, 2018

DOI: 10.1021/acsnano.8b03943
ACS Nano 2018, 12, 11860−11870

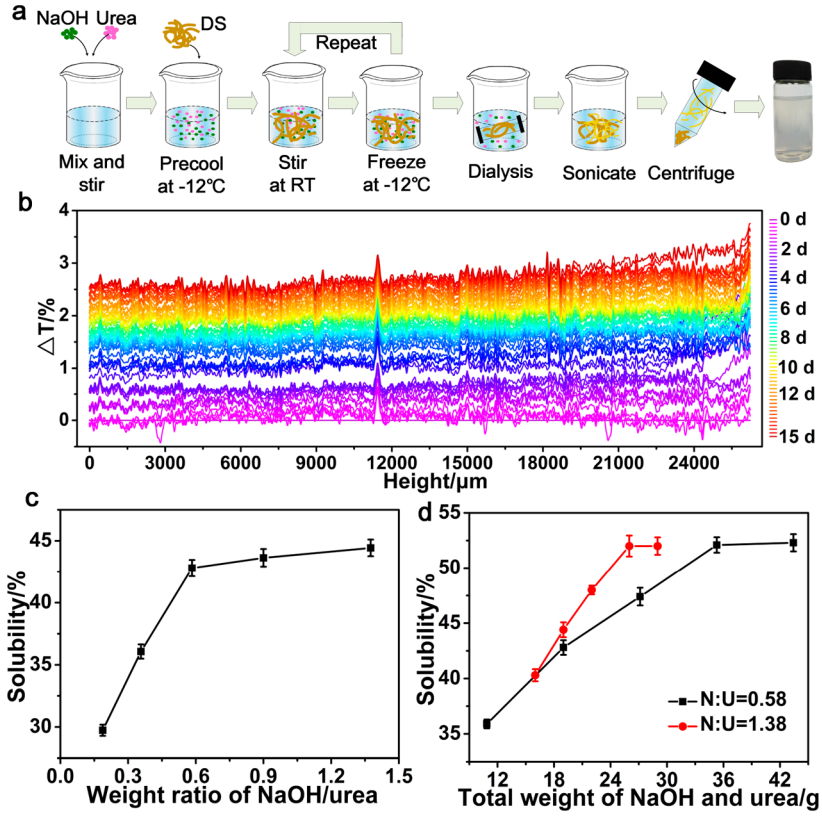

Figure 1. Schematic diagram and experimental results showing the preparation, stability, and solubility of silk nanoribbons (SNRs). (a) Schematics showing the preparation of SNRs by partially dissolving silk using the NaOH/urea system at −12 °C. (b) Referenced transmittance history of SNRs suspension (N:U = 0.19) from 0 to 15 d, illustrating the stability of SNRs suspension. The suspension was scanned along the height from the bottom to the top of the suspension (*x* axis). To enhance variations, transmittance variation (ΔT/%) was acquired by subtracting the first transmittance profile to all other profiles. The solubility diagrams of DS in NaOH/urea solution at (c) different weight ratios of NaOH to urea, and (d) different total weight of NaOH and urea (the total weight of NaOH and urea in b and c was 19 g; "N:U" represents the weight ratio of NaOH to urea).

ability to destroy hydrogen bonds and thus can maintain the nanofibril structures from natural silk in the dissolution step. The width of SNFs obtained by this method ranges from 10 to 120 nm, but their thickness has not been studied.[17,18,20,36,37] The silk fibers exfoliated from the natural silk have exhibited excellent properties, as typically seen in the silk-based materials.[16] However, there are several limitations in the top down method. For example, SNFs obtained from the FA-$CaCl_2$ solvent system could not maintain a solution state in all-aqueous environments;[20,36,38,39] the SNFs suspension obtained from the FA-LiBr solvent system must be stored at 4 °C before use to avoid gelation,[36] and HFIP is a toxic solvent and harmful to the ecological environment.[16] Furthermore, the relationships among the silk hierarchical structure, process, and the resulting morphology (dimension and structure) of resulting SNFs have not been fully understood. In general, none of the above methods truly takes advantage of the basic building block of silk fiber, which might be the key for fabricating silk-based materials with outstanding properties.

The use of mixed alkali/urea systems (*e.g.*, sodium hydroxide (NaOH)/urea, lithium hydroxide/urea, and potassium hydroxide/urea system) to dissolve cellulose, chitosan, or chitin at low temperatures has been well documented.[40−43] For example, Zhang et al. first demonstrated that the NaOH/urea system is a highly effective and nontoxic solvent for dissolving cellulose at −12 °C and the approach can be used to prepare a homogeneous cellulose solution.[44−47] This is because when cellulose is immersed in the precooled NaOH/urea solvent, the hydrogen-bonded network structure between the cellulose macromolecules and small molecules in the solvent can rapidly form an inclusion complex, bringing cellulose into the aqueous solution.[48] As both silk and cellulose molecules have strong hydrogen bonds, where the dissolution treatment is essentially a dissociation process to destroy hydrogen bonds, we hypothesized that the alkali/urea solvent system might also be suitable to dissolve silkworm silk.

The goal of this study was to explore whether stable SNFs solution or suspension could be obtained using the NaOH/urea solvent system. Surprisingly, we discovered that the NaOH/urea solvent did not fully dissolve silkworm silk, but it could exfoliate them into nanoribbon-like SNFs with thickness similar to that of single β-sheet layer. The discovered single-layered SNFs may represent the building blocks of native silk fibers, and they are termed silk nanoribbons (SNRs) in this study. The structure and processing relationships of SNRs were carefully studied by transmission electron microscopy (TEM), atomic force microscopy (AFM), and solution small-angle X-ray scattering (SAXS), and they were also correlated with the initial silk hierarchical structure. We speculate that SNRs have great potential to prepare high-performance silk-based materials, such as films, gels, silks, and scaffolds for many advanced applications, such as biosensing devices, optics, photonics, tissue engineering, biomedicines, or energy storage.

DOI: 10.1021/acsnano.8b03943
ACS Nano 2018, 12, 11860−11870

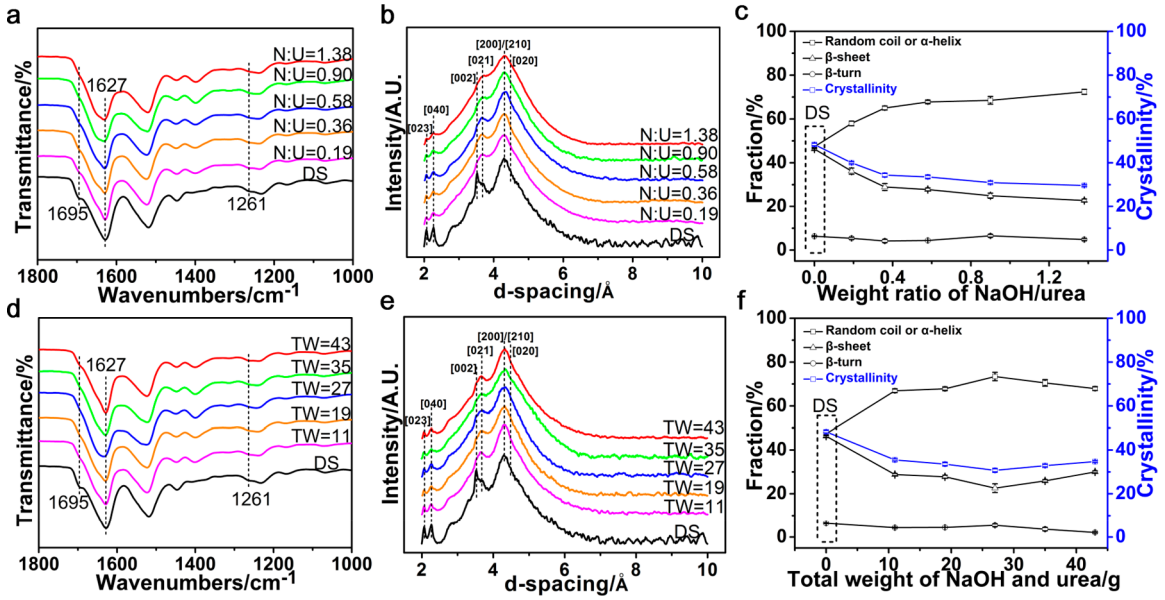

Figure 2. Molecular and crystalline structure characterization of a freeze-dried suspension containing silk fibroin and SNRs. (a,d) Fourier transformed infrared (FTIR) spectra of a freeze-dried suspension to confirm the molecular structures. (b,e) 1D SR-WAXD profiles of freeze-dried suspension. (c,f) Crystallinity and secondary structure content of the freeze-dried suspension. The suspension was derived from the NaOH/urea solution (a−c) at different weight ratios and (d−f) at different total weight of NaOH and urea. (a−c) The total weight was 19 g. (d−f) The weight ratio of NaOH to urea was 0.58. "N:U" represents the weight ratio of NaOH to urea. "TW" represents the total weight of NaOH and urea.

RESULTS AND DISCUSSION

"Solubility" Evaluation. With NaOH and urea mixed at different weight ratios (*i.e.*, 0.19, 0.36, 0.58, 0.9, and 1.38) and the total NaOH and urea weight kept at 19 g to form the solvent system, a homogeneous silk suspension could be obtained after the steps of dissolution (or exfoliation), dialysis, sonication, and centrifugation (Figure 1a). The last image in Figure 1a is the optical image of the SNRs suspension, which exhibited a homogeneous liquid without obvious precipitation. To further characterize the stability of this SNRs suspension, several light transmission experiments were performed. The transmittance variation ($\Delta T/\%$) of the SNRs suspension at different height (Figure 1b) was basically the same, where this horizontal spectrum was referred as the baseline ($\Delta T\% = 0$). With an increase in aging time, the transmittance variation was found to increase. However, the increase was found to be very small. For example, after 15 d of aging, the transmittance variation at different heights increased only by about 3.5%, which indicated that the suspension was still uniformly dispersed. In other words, the suspension was stable without aggregation of SNRs after 15 d of aging at 25 °C. The diagram of DS solubility (or the weight ratio of extracted SNRs to the initial DS content) as a function of weight ratio of NaOH to urea is shown in Figure 1c, which showed that an increase in SNR was obtained with increasing NaOH/urea ratio, but the solubility reached a plateau value at around 45% when the NaOH/urea ratio surpassed 0.6. In a separate study, the solubility of DS was measured as a function of the total NaOH and urea weight at two different NaOH and urea ratios (*i.e.*, N:U = 0.58 and 1.38, respectively). The results are illustrated in Figure 1d, where the solubility was found to increase with the total NaOH and urea weight. In this figure, it was seen that the solubility reached a similar maximum value (around 52%) for both solvent systems at two different NaOH and urea ratios, whereby the higher NaOH content system required less total NaOH and urea weight. Zhang et al. reported the dissolution mechanism of cellulose in the NaOH/urea system.[48−50] In the system of cellulose/NaOH/urea, NaOH "hydrates" was attracted to cellulose chains through the formation of new hydrogen-bonding networks at low temperatures, while urea hydrates could self-assemble at the surface of the hydrogen-bonded cellulose with NaOH to form an inclusion complex, leading to the dissolution of cellulose. As both silk and cellulose molecules have strong hydrogen bonds, NaOH "hydrates" might also be attracted to fibroin chains through the formation of new hydrogen-bonding networks in the exfoliating process of DS. However, the interactions between urea and fibroin may be different from the interactions between urea and cellulose. In Deyoung et al.'s work, at lower urea concentration (less than 3 mol/L, the denaturation midpoint), the solubility of apomyoglobin, a kind of protein, decreased with the increase in urea concentration because the urea-induced predenaturation conformational change would expose the hydrophobic surface.[51] Urea could react with the hydrophilic polar side chains of amino acid and form hydrogen bonds, and this would not destroy hydrogen bonds of the hydrophobic intrachains.[52] In most of our experiments, the molar content of urea was also less than 3 mol/L. Therefore, we speculate that NaOH has a stronger ability than urea to partially destroy both intra- and intermolecular hydrogen bonds in silk fibroin molecules with the aid of hydroxyl group. As a result, the higher NaOH content system required less total NaOH and urea weight. Furthermore, the NaOH content has a much larger effect on the solubility of DS or the ability to extract SNRs using the NaOH/urea solvent system. Through the addition of the "rinse" process before sonication, completely dissolved silk fibroin molecules were removed, and the yield of SNRs was calculated. When the solubility was near the minimum value at about 30.4%, the yield of SNRs, which was obtained from the

DOI: 10.1021/acsnano.8b03943
ACS Nano 2018, 12, 11860−11870

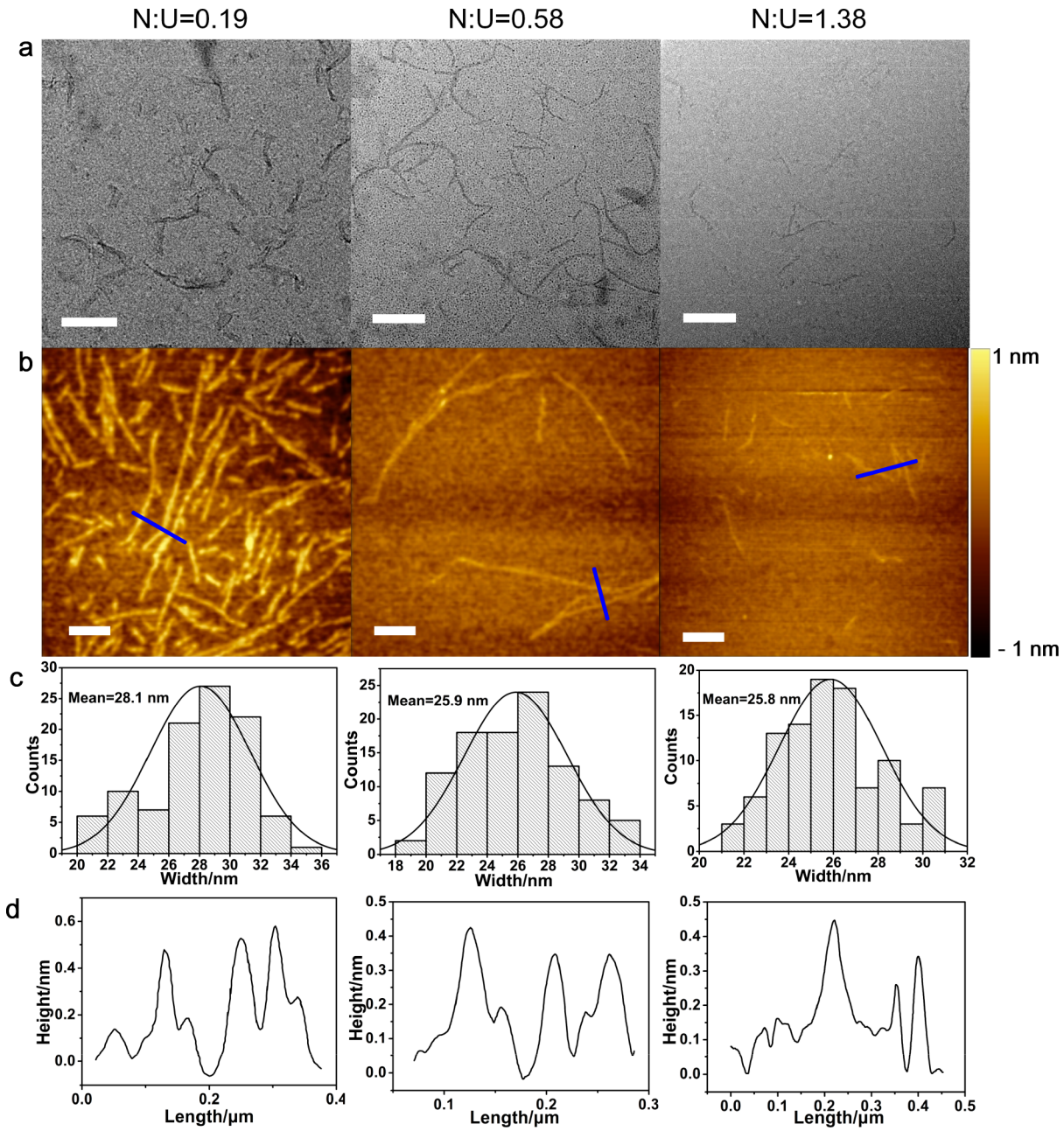

Figure 3. Characterization of morphology and size of SNRs. (a) TEM images, (b) AFM images, (c) the width distribution of SNRs from AFM images, and (d) the height profile of SNRs from AFM measurements. SNRs were derived from the NaOH/urea solution at different weight ratios, and the total weight was 19 g. "N:U" represents the weight ratio of NaOH to urea. Scale bars = 200 nm. The blue lines in (b) were used to measure the (d) height of three SNRs. Two typical AFM images used for the width distribution analysis were shown in SI, Figure S5.

NaOH/urea system (weight ratio of NaOH to urea, 0.19; total weight of NaOH and urea, 19 g), was about 21.4%.

Molecular and Crystalline Structures of SNRs. The molecular and crystalline structures of a freeze-dried suspension, containing silk fibroin and SNRs, were investigated by Fourier transform infrared spectroscopy (FTIR) and synchrotron radiation wide-angle X-ray diffraction (SR-WAXD) techniques. The silk fibroin was at the molecular scale, which was obtained by dissolving silk completely, where SNRs were the result of a partial dissolution, or more precisely, exfoliation of silk.

On the basis of previous publications,[19,53] characteristic peaks in FTIR-ATR spectra of silk can be summarized as follows. For amide I, the absorbance peaks at 1697 and 1623 cm^{-1} are due to the β-sheet, and the peaks at 1650 and 1678 cm^{-1} can be assigned to random coil/α-helix and β-turn, respectively. The results from molecular and crystalline structure characterization of a freeze-dried suspension containing silk fibroin and SNRs, using FTIR and WAXD techniques, are shown in Figure 2. In Figure 2a (FTIR spectra of a freeze-dried suspension at different NaOH/urea weight ratios), the spectra peaks from SNRs were found to be slightly changed compared with those from DS. For example, with the increasing weight ratio (while the total weight of NaOH and urea was fixed at 19 g), the peak at 1695 cm^{-1} gradually disappeared and the peak at 1627 cm^{-1} became broader. The conformation contents in the sample could be calculated from the deconvolution of amide I peaks (Supporting Information

DOI: 10.1021/acsnano.8b03943
ACS Nano 2018, 12, 11860−11870

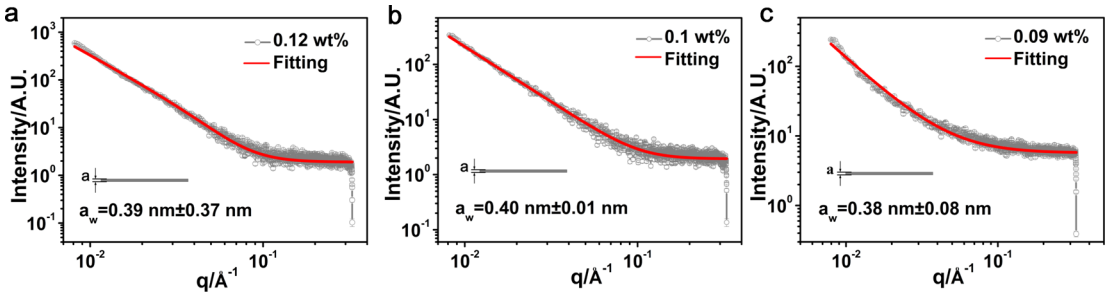

Figure 4. SAXS profiles of SNRs suspension and the fitted curves using the lamellar model in combination with a Gaussian type function. The SNRs suspensions were prepared using the NaOH/urea solution at different weight ratios ((a) 0.19, (b) 0.58, and (c) 1.38), and the total weight was 19 g.

(SI), Figure S1), and the corresponding contents of β-sheet, β-turn, and random coil/α-helix are shown in Figure 2c. It was seen that the β-sheet content of SNRs was lower than that of DS. As the weight ratio increased, the β-sheet content decreased but the random coil/α-helix content increased. However, in Figure 2d, the changing trend of the peaks was found not to be monotonous. For example, in Figure 2f, when the total weight of NaOH and urea increased (the weight ratio of NaOH to urea was fixed at 0.58), the β-sheet content and crystallinity were found to decrease first and then increase. Possible reasons for the above observation might be as follows. When the urea amount was larger than 17 g ($27/(1 + 0.58) \times 1 = 17$ g), the NaOH content ($27 - 17 = 10$ g) was relatively low. The high urea concentration could decrease the permittivity of the solution, enhance the formation and stability of peptide hydrogen bonds, and even influence the unfolding and refolding process of chains. Consequently, the β-sheet content and crystallinity of the freeze-dried SNRs suspension were found to increase slightly.[54,55] However, the β-sheet content of all samples was still lower than that of DS. When the weight ratio of NaOH to urea was 1.38 (SI, Figure S2), the β-sheet content was found to decrease with the increase in the total weight of NaOH and urea. The maximum β-sheet content of freeze-dried samples was 33.5% (Figure 2c).

The crystalline structures of the SNRs were investigated by SR-WAXD. The measured 2D WAXD patterns for the varying samples are shown in Figure S3 (SI), where the integrated 1D WAXD patterns of SNRs and DS are shown in Figure 2b,e (also SI, Figure S2b). It is known that *B. mori* silk has two forms of crystal structure: silk I and silk II, while all WAXD patterns showed that SNRs possessed a silk II structure. In all samples, the main crystalline peak at the d spacing of 0.43 nm could be indexed by the [200]/[210] lattice planes. Compared with the DS sample, the [002] lattice plane at the d of 0.35 nm in SNRs was not obvious, but the [021] lattice plane at 0.37 nm was quite evident. With the increase in the weight ratio or total weight of NaOH and urea, the peak height in [021] lattice plane became smaller. The deconvolutions of the 1D SR-WAXD patterns are shown in SI, Figure S4, which were used to estimate the crystallinity. Parts c and f of Figure 2 (also SI, Figure S2c) show the crystallinity change as a function of the weight ratio and total weight of NaOH and urea, respectively. It was found that the maximum crystallinity of the freeze-dried samples was 40.0% (Figure 2c), while the changing trend of the crystallinity was the same as that of the β-sheet content. This result is expected. As the NaOH concentration increased, the solvent system possessed stronger ability to destroy the hydrogen bonds in DS, and more silk fibroin at molecular scale could appear in the suspension. Thus, a negative correlation should exist between the content of NaOH and the β-sheet content or the crystallinity.

Dimensions of SNRs. To analyze the dimensions of SNRs obtained from different solvents, TEM and AFM techniques were used to examine the solid samples by evaporating water from the suspensions. In addition, AFM was also used to examine the SNRs suspension directly. In these measurements, if the solubility of DS was larger, more SNRs and silk fibroin would be obtained. If the β-sheet content and crystallinity were higher, the weight ratio of SNRs to silk fibroin would be higher and more SNRs were maintained from the dissolution of DS. Three freeze-dried samples of SNRs suspensions were investigated in detail. Parts a and b of Figure 3 show typical TEM and AFM images of SNRs prepared from the NaOH/urea solutions at different weight ratios (*i.e.*, 0.19, 0.58, and 1.38). In Figure 3c, the histogram shows the width distribution measured from multiple AFM images (SI, Figure S5 illustrates other AFM images used to determine the SNR widths). The width distribution of the resulting SNRs was found to be in the range of 26−32, 20−30, and 23−27 nm (their average widths were 28.1, 25.9, and 25.8 nm), derived from the suspensions at NaOH/urea weight ratio of 0.19, 0.58, and 1.38, respectively. It was found that the width of SNRs derived from the lower NaOH/urea weight ratio was wider than that prepared from the higher NaOH/urea weight ratio. Through the AFM measurement in the liquid environment (or in suspension, SI, Figure S6), SNRs were found to possess a width about 31.3 nm. Xu et al.[6] reported that each silk fiber was composed of numerous nanofibrils of a diameter of around 30 nm for *B. mori* silkworm silks through AFM measurements. In our results, the width results of SNRs were consistent with Xu's results.

The thickness of SNRs was also measured from the AFM measurement in the contact mode, where the results are shown in Figure 3d. It was found that SNRs possessed a lamellar (or ribbon) shape, which possessed an average thickness $a = 0.44$ nm with a standard deviation $\sigma_a = 0.08$ nm, an average thickness $a = 0.41$ nm with a standard deviation $\sigma_a = 0.08$ nm, and an average thickness $a = 0.33$ nm with a standard deviation $\sigma_a = 0.03$ nm, from the suspensions at different NaOH/urea weight ratios of 0.19, 0.58, and 1.38, respectively. From the AFM data, the thickness of SNRs is about the same as the distance of the β-sheet layers and interchains in β-crystallite. According to the optical image of SNRs suspension, the WAXD peaks of freeze-dried SNRs, and AFM images, we believe that the SNRs were exfoliated directly from DS, not the result of drying, protein assembly, or other processing. This

DOI: 10.1021/acsnano.8b03943
ACS Nano 2018, 12, 11860−11870

conclusion was further verified by the solution SAXS experiments, as described next.

We note that as AFM samples were prepared by evaporating water from the SNRs suspension, SNRs could aggregate into thicker stacks. To overcome this problem, we have carefully selected the region without the stack formation for the thickness estimate by AFM. To confirm the estimated thickness of SNRs from AFM, solution SAXS was also carried out on three SNRs suspensions using different NaOH/urea weight ratios (*i.e.*, 0.19, 0.58, and 1.38). The measured scattered intensity profiles are shown in Figure 4, which exhibited a completely diffuse feature. As the investigated suspensions are all in the dilute ranges (concn from 0.09 to 0.12 wt %), these scattering profiles are dominated by the form factor of SNRs. A suitable fitting model was chosen to fit the scattering results. As SNRs can be considered infinitely long (several hundreds of nanometers, outside the SAXS detection limit), and its width (mean value >25.8 nm) is substantially larger than its thickness (mean value around 0.4 nm from AFM), we have used a simplified polydisperse lamellar model to describe the SAXS intensity profiles of SNRs in suspension. The ribbon model containing comparable width and thickness dimensions was also used to fit the data, but the result was not reasonable. The analytical form of 1D SAXS data using the simple lamellar model can be given by the following equation.[56]

$$I(q) = 2\pi \frac{2\Delta\rho^2[1 - \cos(q\delta)]}{\delta q^4} \quad (1)$$

where $I(q)$ is the scattered intensity, δ is the thickness of the lamella, q is scattering vector, $\Delta\rho$ is the density contrast ($= D_{\text{lamella}} - D_{\text{solvent}}$), where D_{lamella} and D_{solvent} are the density of the lamella and solvent, respectively. This lamellar model contains only four parameters: the SNR thickness, polydispersity (assuming a Gaussian distribution), background, and a scaling factor. By adjusting the background, scaling factor and polydispersity, the SNR thickness was extracted by fitting the experimental data. As the fitting profile and the experimental line exhibited high confidence in the chosen q range (dominated by the SNR cross-section), the estimated SNR dimension probably reflected a good thickness estimate in the suspension state. The fitted profiles and their corresponding parameters (thickness and variance) are shown in Figure 4. It was found that this model fit the curves quite well, except for the low q region (<0.01 $Å^{-1}$). This is expected, as the scattered intensity at the low q region is dominated by the larger scatter dimensions (such as width and even length). From the fitting results, all thickness values of SNRs were about 0.39 nm, very close to the AFM measurements. This value also corresponds well with the height of a single β-sheet layer. The SAXS and AFM results confirmed that the chosen NaOH/urea solvent at low temperature is able to extract the basic building blocks, or SNRs, from silkworm silk.

Simulation of Disruption of Silk Fibroin Crystal Structure in NaOH/Urea Solution. Silk consists of secondary structures such as random coil, α-helix, β-turn, and β-sheet, where the β-sheet crystalline structure is the most difficult to be dissolved in solvents. The β-sheet crystalline structure possesses a polar arrangement with glycine side chains (−H) in the front face of the β-sheet projection and alanine side chains ($-CH_3$) in the back face.[57] The β-crystalline structure is stacked through van der Waals (VDW) interactions by β-sheets, having similar front-to-front or back-to-back faces.[57,58] The intersheet distances between the front-to-front and back-to-back stacking are 0.37 and 0.55 nm, respectively.[57,58] The interchain distance between the β-sheets, governed by hydrogen bonds, is about 0.5 nm.[57]

Although hydrogen bonds are recognized as stronger than the VDW interactions, the collective VDW force between regular structures can be comparable with that of hydrogen bonds. To understand the dissolution process of silk β-sheet nanocrystal in NaOH/urea solution at −12 °C, two series of molecular dynamics simulations were carried out to verify whether the thickness of SNRs is intersheet or interchain distance. The chosen model (SI, Figure S7a) was created through a typical silk crystal structure. Figure 5a shows the VDW interactions and hydrogen bonds packing directions, and Figure 5b illustrates the periodic boundary connections of infinite fibril models. In the simulation, the upper two layers of the silk fibroin crystal structure was dragged apart by an

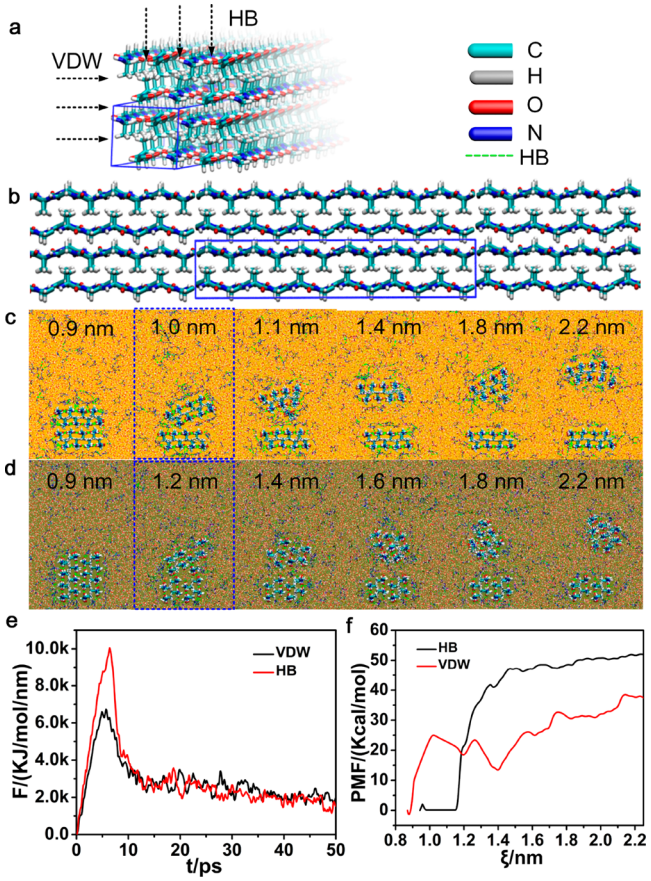

Figure 5. Simulation model, snapshots of deformation, force-time profiles, and potential of mean force (PMF)-displacement profiles. (a) Replication of the unit cell into a 16-chain system. (b) Molecular structure of silk fibroin chains in crystal and their periodic connections as infinite models used for the simulation. The equilibrium structures of the umbrella sampling for destroying (c) hydrogen bonding (HB) and (d) van der Waals (VDW) interactions. The data in (c) and (d) are the distances between centers of mass of the two parts during umbrella sampling runs for the disruption of HB and VDW interactions, respectively. (e) The force required to break the HB and VDW interactions during the pulling process. (f) The corresponding PMF calculated through the weight histogram method for the disruption of the crystal structure.

DOI: 10.1021/acsnano.8b03943
ACS Nano 2018, 12, 11860−11870

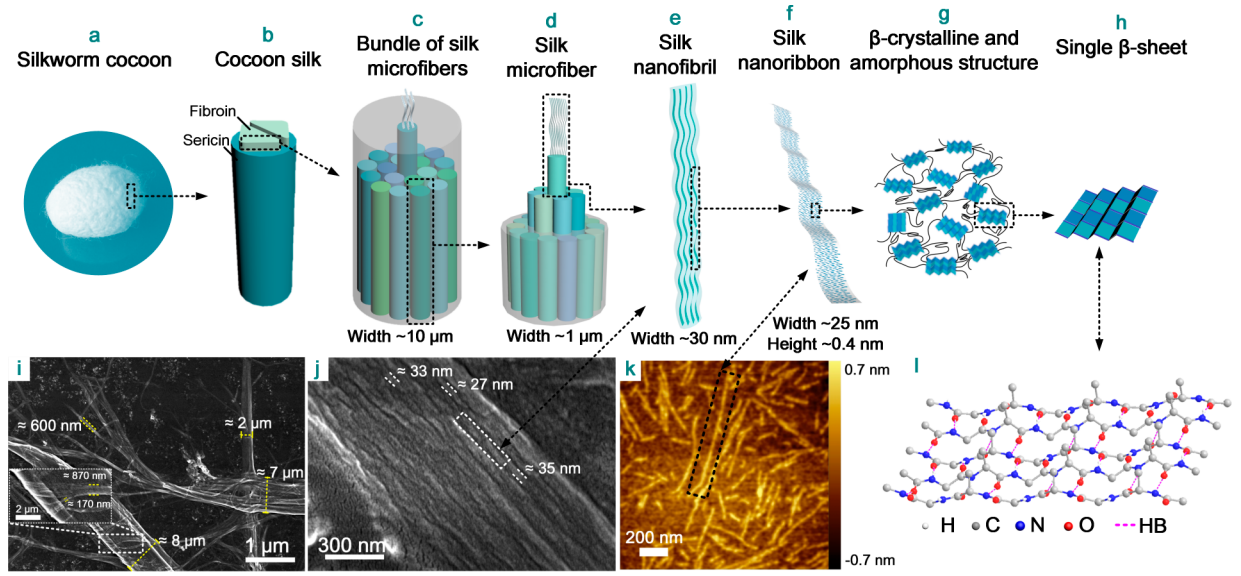

Figure 6. Proposed hierarchical structure of silk. (a) Silkworm cocoon. (b) Model of cocoon silk, containing sericin and fibroin. (c) Model of DS, containing a bundle of silk microfibers. (d) A single silk microfiber (the width is about 1 μm). (e) The SNF (the width is about 30 nm) in a microfibril. (f) The SNR in a nanofibril. (g) The structure of SNR consisting of β-sheets and amorphous structure. (h) The structure of a single β-sheet. (i,j) SEM images of the mixture after dialysis obtained by dissolving in the NaOH/urea solution. DS was exfoliated and form microfibers from two terminals, while the microfiber is composed of oriented SNFs. (k) AFM image of SNRs. The width of SNRs is about 25 nm, and the height of SNRs is about 0.4 nm. (l) Atomic structure of single β-sheet layer.

umbrella potential with the force constant of 100 kcal/mol/Å^2, while the lower two layers remained constraint. The initial crystal silk fibroin model was positioned in two directions for the measurement of VDW (SI, Figure S7b) and hydrogen bond (SI, Figure S7c) breaking interactions, respectively.

In the simulation, the initial distances between the centers of mass of the upper and lower two β-sheet layers and the β-sheet chains were 0.87 and 0.94 nm, respectively. The short pulling runs were used to estimate the force required to break the crystal structures. Parts c and d of Figure 5 show snapshots of the equilibrium structures after each umbrella sampling runs for the disruption of HB and VDW interactions, respectively. It was found that the maximum force of breaking HB and VDW interactions were 10000 and 6500 kJ/mol/nm, respectively. Thus, the force required to break the HB interactions was 40% larger than that for the VDW interactions between layers (Figure 5e). Intermediate structures during the pulling process were used for further umbrella sampling calculations. The potential of mean force (PMF) obtained from the umbrella sampling can describe the free energy needed to disrupt the crystal structure along the corresponding directions. It was found that the disruptions were not straightforward, and struggling of interactions was frequently noticed at small separations. In specific, for HB interactions, the pulled structure could revert back to the original structure after equilibration at interstrand distances below ~1.2 nm. As shown in Figure 5f, the deformation of VDW was possible below 1.2 nm, but the long-range interactions could exist leading to a nonsmooth curve. The PMF curves also showed that breaking hydrogen bonds required much more energy, where this process was much harder than that of VDW interactions. In Figure 5c, hydrogen bonds, illustrated in green dashed lines, showed that after the disruption of VDW interactions, the urea molecules were able to form competitive HBs with the peptide backbone, which could facilitate the disruption of the regular crystal structures. The HBs between urea and silk fibroin after dragging the two slices apart might lead to solvation of the crystal while the dragging apart of hydrogen bonds did not make much difference to the regular HB packing between the strands. Thus, the single β-sheet layer (or SNRs) could be maintained easily. This indicated that the exfoliated SNR can be considered as the basic building block to construct hierarchical silk structure.

Hierarchical Structure of Silk. Historically, the semicrystallite model has been used to explain the structure of silk. It was commonly recognized that silk fibers are considered as a composite material, in which β-crystallites are embedded in the amorphous matrix.[59,60] Several different models have been proposed to describe the silk hierarchical structure at different scale. For example, on the basis of AFM images of the silk surface and cylindrical fibrils having diameters about 90−170 nm, the "fibrillar" model with multilevel organizations has been proposed for spider and silkworm silk fibers.[61] Separately, the "string of beads" model was proposed by Porter et al. to describe the spider silk structure, where each fold contains six peptide segments.[62,63] With this model, the authors explained how the degree of ordered phase could affect the mechanical properties of spider silk fibers. Some other researchers also used the "fringe-micelle" model to describe the formation of SNFs,[64−66] as a result of coalescence of micellar structure upon elongation. It was interesting to note that Xu et al. reported each *B. mori* silk fiber consists of many nanofibrils with cross-sectional dimension about 30 nm, where these nanofibers are in fact spirally twisted belts.[6] Although these models have been created to describe the multilevel structures of silk fibers based on microscopic measurements (*e.g.*, AFM, SEM, and TEM) or theoretical consideration,[67,68] many of these models lack systematical experimental support.[5]

According to the dimensional information on SNRs extracted using the NaOH/urea solution, we propose a hierarchical structure model that is shown in Figure 6. Figure 6a represents the silkworm cocoon. In a typical cocoon, two

DOI: 10.1021/acsnano.8b03943
ACS Nano 2018, 12, 11860−11870

fibroin brins are coated with sericin, forming the cocoon silk (Figure 6b). The fibroin brin is made up of a bundle of silk microfibers (Figure 6c). It is seen from Figure 6i, in the dissolving process, the two brins of DS can be exfoliated and become microfibers with the diameter about a few hundred nanometers to one micrometer. The silk microfiber (Figure 6d) is composed of oriented SNFs (Figure 6j) with a diameter about 30 nm. The SNF is composed of the assembly of SNR having a uniform thickness about 0.4 nm and a width ranging from 20 to 32 nm. In the SNF, SNRs are stacked along the nanofiber direction (Figure 6e). The SNR (Figure 6f,k) contains β-crystalline and amorphous phases (Figure 6g). In the β-sheet crystallites with a polar-antiparallel arrangement, the intersheet distances between two glycine faces (front-to-front) or two alanine faces (back-to-back) are 0.37 and 0.55 nm, respectively.[57] The thickness of the SNR is about 0.4 nm, having the same thickness as a single β-sheet layer. The β-crystalline structure is composed of many single β-sheets (Figure 6h), where the atomic structure diagram of the β-crystalline structure is shown in Figure 6l.

SNRs Membrane. As the basic building blocks of silk fiber, SNRs can be reassembled artificially to fabricate a different kind of silk-based materials. As shown in Figure 7, both SNRs

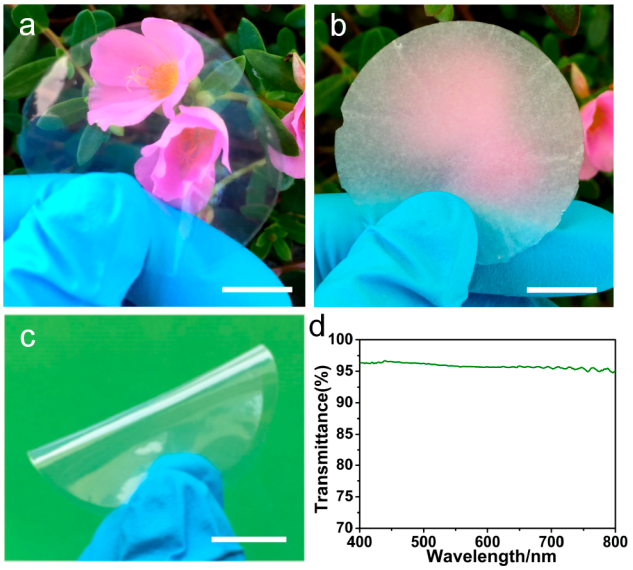

Figure 7. (a) Image illustrating the transparent SNRs optical membrane. (b) Image illustrating the opaque silk microfibers (SMFs) membrane. (c) Image illustrating the flexibility of SNFs membrane. (d) UV−vis transmittance of SNRs membrane. Scale bars = 1 cm.

and silk microfibers (SMFs) membranes were prepared by vacuum filtration. Compared with conventional SMRs membrane (Figure 7b), SNRs membrane with a thickness about 10 μm (Figure 7a) was near optically transparent (about 95%) (Figure 7d) throughout the visible light region (400−800 nm), while SMRs membrane was not. In addition, SNRs membrane also exhibited excellent flexibility (Figure 7c) and insolubility (SI, Figure S8) in common solvents.

CONCLUSIONS

In this study, we demonstrated a top-down approach to exfoliate the silk fibers into nanoribbons, instead of dissolving them into silk fibroin molecules, using the NaOH/urea solution at a low temperature (−12 °C). The exfoliated SNRs are a 2-D assembly containing a single molecular layer with thickness about 0.4 nm, containing both single β-sheet layers and amorphous chains. The existence of the ultrathin SNRs with a single molecular layer from silk fibers has never been reported before. In the extraction process, the NaOH/urea solution was able to destroy the VDW force between the molecular layer while maintaining the integrity of SNRs structure (without disturbing the hydrogen bonds with the layer) at −12 °C. On the basis of the computer simulation results and the existence of SNRs from AFM and SAXS measurements, a hierarchical structure for silk fibers was proposed. In this model, the basic building block in the smallest nanofibril of silkworm was found to be of a ribbon shape with the thickness of about 0.4 nm. We speculate that through the self-assembly or ordered construction, SNRs can be used as reinforcing agents or direct new building element to regenerate silk-based materials with outstanding mechanical properties or functionality for a wide range of applications such as tissue engineering scaffolds, surgical sutures, ultrathin membrane. or transparent flexible film for filtration, optics, photonics, or bioelectronic interfaces. The findings in this study offered a perspective for the fabrication of silk-based materials with high performance.

METHODS

Preparation of SNRs Suspension. DS was prepared according to the procedure published earlier.[69] Cocoons were boiled 2 times for 30 min in an aqueous solution of 0.5% (w/v) sodium carbonate and then rinsed thoroughly with deionized water to remove sericin and residual sodium carbonate. A mixed solution based on NaOH/urea/H_2O (100 g) at different mass ratio was precooled to −12 °C. The DS sample (3 g) was then dispersed into the solvent system. The suspension was stirred for 10 min every 12 h over 3 days. The recovered suspension was dialyzed in a semipermeable cellulose membrane (molecular weight cutoff (MWCO) = 7000 kDa) for 3 days. The final mixture was sonicated in ice−water at 300 W. After 30 min of sonication, the SNRs dispersion was harvested by centrifugation at 4500 rpm for 20 min. The dispersion was transparent and milky liquid. After the centrifugation of silk mixture, precipitates were dried in oven at 60 °C. The weight of dried centrifugal precipitates was w_1. The weight of DS added in the beginning of experiment was 3 g. As shown in eq 2, the solubility of DS (w) was calculated as follows.

$$w = 1 - w_1/3 \times 100\% \quad (2)$$

To determine the yield of SNRs, rinsing was performed on the SNRs suspension to remove water-soluble silk fibroin molecules after the dialysis. After further sonication and centrifugation of silk mixture, the SNRs suspension was acquired prior to lyopilization. As the initial DS weight before dissolution was 3 g and the weight of freeze-dried SNRs was w_2, the yield of SNRs w' was calculated according to eq 3.

$$w' = w_2/3 \times 100\% \quad (3)$$

Preparation of SNRs and SMFs Membranes. The SNRs and SMFs membranes were prepared by using the SNRs/SMFs suspensions in combination with a vacuum filtration setup (pressure ~0.1 MPa) and polycarbonate filtration membranes (pore size ~200 nm; diameter was 4.7 cm; Millipore).

Stability of SNRs Suspension by Light Transmission Measurement. The physical stability of SNRs suspension was analyzed by a Multi Sample Stability Analyzer (Turbiscan TOWER, Formulaction Co., L'Union, France). In this instrument, sample scanning was carried out from the bottom to the top of the suspension in a special cuvette holder. The measurement was conducted at 25 °C for 15 days. The system contained a pulsed near-infrared light source (λ = 880 nm) and two synchronous detectors. The transmission

DOI: 10.1021/acsnano.8b03943
ACS Nano 2018, 12, 11860−11870

detector (at 180°) received the transmission light through the sample, while the backscattering detector (at 45°) detected the scattered light from the sample. The system scanned the entire height of the sample, collecting both transmission and backscattering data at an interval of 40 μm position change.

FTIR Spectroscopy of Freeze-Dried Samples. The SNRs suspension was freeze-dried to prepare samples for the FTIR measurement. The FTIR spectra were obtained using a Nicolet 8700 spectrometer equipped with an ATR (attenuated total reflectance) accessory and a diamond crystal (ATR Smart Performance module) in the spectral region of 525−4000 cm^{-1} by accumulating 32 scans at a resolution of 4 cm^{-1}. Data analysis was performed by the software PeakFit V4.12 (SeaSolve Software, Inc.). A baseline was subtracted from the spectra. The amino I of FTIR spectra were fitted using four peaks, including random coil and α-helix at 1640−1660 cm^{-1}, β-turn at 1660−1690 cm^{-1}, β-sheet at 1620−1640 cm^{-1}, and antiparallel β-sheet at 1690−1700 cm^{-1}.

SR-WAXD Research of Freeze-Dried Samples. The suspension was freeze-dried to prepare samples for SR-WAXD measurements. 2D SR-WAXD patterns were collected at the 15U Beamline, equipped with a Rayonix-165 detector in the Shanghai Synchrotron Radiation Facility. The freeze-dried samples of suspension were carefully sandwiched between two pieces of Kapton tape to prevent any preferred orientation effect. Background measurements were performed using two pieces of Kapton tape. The chosen radiation wavelength was 0.0775 nm and the beam spot size was 0.8 × 0.8 μm^2. The distance of sample to detector was 17.3 cm, and the exposure time was 30 s. FIT2D (V12.007) was used to process SR-WAXD patterns. The degree of crystallinity was obtained using the software PeakFit V4.12 (SeaSolve Software, Inc.), in which the diffraction profile was deconvoluted. The degree of crystallinity was obtained via the ratio of I_c to $I_c + I_a$, where I_c is the area of the integrated intensities of crystalline peaks, while I_a is the area of the integrated intensity of the amorphous halo.

SR-SAXS Measurement of SNRs Suspensions. The SR-SAXS measurements of SNRs suspensions were carried out at the Beamline 16B of the Shanghai Synchrotron Radiation Facility. In this experiment, 2 mL suspension was pump into a glass capillary through the syringe pump. To reduce the radiation damage,[70] the sample was allowed to flow continuously through the glass capillary during the measurement. The chosen radiation wavelength was 0.124 nm, and the beam spot size was 0.8 × 0.8 μm^2. The distance of sample to detector was 2.21 m, covering a q (scattering vector) range from ∼0.008 to ∼0.327 $Å^{-1}$, and the exposure time was 300 s. The data analysis was performed using the software XPolar 1.4.9.0 (Precision Works NY, Inc.). Then 1D SAXS data fitting was performed using the fitting subroutine implemented in the Sasview 3.1.2 package (GitHub Inc.), with customized model construction function using a lamellar model with a Gaussian type function.

TEM and AFM Measurements. For TEM sample preparation, a SNRs suspension was first diluted to 0.01 mg/mL by deionized water and then dropped onto a carbon-film-coated copper grid. After 2 min of sample deposition, the excess liquid was absorbed by filter paper. The specimen was observed by TEM (JEOL JEM-2100, Japan) at a voltage of 200 kV.

For AFM (Agilent 5500) measurements in the solid phase, samples were prepared by depositing the SNRs suspension (0.001 mg/mL) onto a freshly cleaved mica substrate. The tapping mode AFM imaging was used at a scanning range of 5 μm and a scanning speed of 1 Hz. From the AFM images, the widths of the nanofibrils were measured using the Nano Measurer 1.2 software. The statistical width was acquired based on the measurements of 100 nanofibrils on AFM images. For AFM measurement in the liquid phase, the morphology of SNRs in suspension (0.3 mg/mL) was observed using a different AFM instrument (Dimension Icon & FastScan Bio) in air. In this measurement, the sample was directly dropped onto the freshly cleaved mica surface. In this measurement, a 100 μm long silicon cantilever having the force constant of 3 N/m was used in the tapping mode at a 0.98 Hz scan rate.

SEM Measurement. The SNRs mixture after dialysis was deposited onto a sample stage using conductive adhesive prior to air drying. The dried samples were subsequently sputtered with platinum and observed using a SEM instrument (Hitachi S-4800) at 5 kV.

Computer Simulations. Molecular dynamics simulations were performed on the typical silk protein (PDB 2SLK) with sequence (GAGAGA···). The original structure was made periodic along the chain axis, as shown in Figure 5, and twice the original size (∼4.2 nm) was used through replicating the chains along the chain axis. The unit cell was also replicated in the other directions (Figure 5b) and the final 16 periodic chains were placed in two directions close to the bottom of a rectangular box of 4.2 × 4.2 × 6 nm^3 (SI, Figure S3).

After the energy minimization of the protein structure, 178 urea molecules and 50 NaOH in their ionic states were added for consistency with experiments. The systems were subsequently solvated in around 3000 water molecules, represented by the TIP3P water model. Thousands of steps of energy minimization were performed before 10 ns equilibration of the whole system with the α-carbon atoms in the proteins constraint. The steered molecular dynamics run followed by a spring constant of 100 kcal/mol/$Å^2$ on the center of mass of the upper two layers, during which the bottom two layers were constraint. The sampling spacing of 0.05−0.2 nm was implemented to generate the intermediate structures for the umbrella sampling runs. Each intermediate run extended for 2 ns and the later 1 ns was taken for data collection. The PMF was calculated through the weighted histogram analysis method.

The temperature was coupled to 261 K using the velocity rescaling method and the pressure was coupled to 1 atm using the Berendsen method. A twin-range cutoff scheme was implemented between 1.2 and 1.4 nm for the nonbonded interactions, and the particle mesh Ewald method[71] with a Fourier spacing of 0.1 nm was applied for the long-range electrostatic interactions. All covalent bonds with hydrogen atoms were constraint using the LINCS algorithm.[72] All MD calculations and system building were performed using the GROMACS[73] molecular dynamics simulation package version 5.0, with the CHARMM36 force field.[74]

ASSOCIATED CONTENT

Supporting Information

The Supporting Information is available free of charge on the ACS Publications website at DOI: 10.1021/acsnano.8b03943.

Deconvolution of FTIR spectra in amide I band; crystalline structure and secondary structure of freeze-dried suspension containing silk fibroin and SNRs; two-dimensional SR-WAXD patterns of freeze-dried suspension containing silk fibroin and SNRs; deconvolution of one-dimensional SR-WAXD pattern; AFM images of SNRs in the solid phase; characterization of morphology and size of SNRs in the liquid phase; silk model of antiparallel β-sheet nanocrystal for molecular dynamics simulation; SNRs membrane immersed in water at room temperature to illustrate the insolubility (PDF)

AUTHOR INFORMATION

Corresponding Authors

*E-mail: zyp@dhu.edu.cn.
*E-mail: wurl@dhu.edu.cn.
*E-mail: benjamin.hsiao@stonybrook.edu.

ORCID

Suna Fan: 0000-0001-6508-360X
Benjamin S. Hsiao: 0000-0002-3180-1826
Yaopeng Zhang: 0000-0002-7175-6150

DOI: 10.1021/acsnano.8b03943
ACS Nano 2018, 12, 11860−11870

Present Address

[§]Q.P.: School of Life Sciences and Biotechnology, Shanghai Jiao Tong University, Shanghai 200240, China.

Author Contributions

Prof. Yaopeng Zhang conceived and directed the research. Miss Qianqian Niu fabricated the SNRs and performed the AFM, TEM, FTIR, WAXD, and SAXS measurements and analyzed all of the data. Prof. Benjamin S. Hsiao, Li Lu, and Dr. Suna Fan joined the SAXS analysis of SNRs. Prof. Rongliang Wu performed the computer simulations. Dr. Qingfa Peng analyzed the structure of SNRs. Prof. Huili Shao and Prof. Huihui Zhang directed the analyses of WAXD.

Notes

The authors declare no competing financial interest.

ACKNOWLEDGMENTS

This work is supported by the National Natural Science Foundation of China (21674018, 21304017), the National Key Research and Development Program of China (2018YFC1105802/2018YFC1105800, 2016YFA0201702/2016YFA0201700), "Shuguang Program" supported by Shanghai Education Development Foundation and Shanghai Municipal Education Commission (15SG30), and the Programme of Introducing Talents of Discipline to Universities (no. 111-2-04). B.S.H. thanks for financial support from the Polymer Program, Division of Materials Research, National Science Foundation in the U.S. (DMR-1808690). The authors also thank Dr. L. Geng and Dr. C. Zhan for their valuable discussion about SAXS data analysis.

REFERENCES

(1) Grubb, D. T.; Jelinski, L. W. Fiber Morphology of Spider Silk: The Effects of Tensile Deformation. *Macromolecules* **1997**, *30*, 2860−2867.

(2) Valluzzi, R.; Jin, H. J. X-Ray Evidence for a "Super"-Secondary Structure in Silk Fibers. *Biomacromolecules* **2004**, *5*, 696−703.

(3) Trancik, J. E.; Czernuszka, J. T.; Bell, F. I.; Viney, C. Nanostructural Features of a Spider Dragline Silk as Revealed by Electron and X-Ray Diffraction Studies. *Polymer* **2006**, *47*, 5633−5642.

(4) Riekel, C.; Madsen, B.; Knight, D.; Vollrath, F. X-Ray Diffraction on Spider Silk during Controlled Extrusion under a Synchrotron Radiation X-Ray Beam. *Biomacromolecules* **2000**, *1*, 622−626.

(5) Du, N.; Yang, Z.; Liu, X. Y.; Li, Y.; Xu, H. Y. Structural Origin of the Strain-Hardening of Spider Silk. *Adv. Funct. Mater.* **2011**, *21*, 772−778.

(6) Xu, G.; Gong, L.; Yang, Z.; Liu, X. Y. What Makes Spider Silk Fibers So Strong? From Molecular-Crystallite Network to Hierarchical Network Structures. *Soft Matter* **2014**, *10*, 2116−2123.

(7) Yuan, B.; Li, J. L.; Liu, X. Y.; Ma, Y. Q.; Xu, H. Y. Critical Behavior of Confined Supramolecular Soft Materials on a Microscopic Scale. *Chem. Commun.* **2011**, *47*, 2793−2795.

(8) Yuan, B.; Li, J. L.; Liu, X. Y.; Ma, Y. Q.; Wang, Y. J. Size Invariance of Fibrous Networks of Supramolecular Soft Materials during Formation under Critical Volume Confinement. *Soft Matter* **2012**, *8*, 5187−5193.

(9) Chen, Z.; Zhang, H.; Lin, Z.; Lin, Y.; Van Esch, J. H.; Liu, X. Y. Programing Performance of Silk Fibroin Materials by Controlled Nucleation. *Adv. Funct. Mater.* **2016**, *26*, 8978−8990.

(10) Lin, N.; Liu, X. Y. Correlation between Hierarchical Structure of Crystal Networks and Macroscopic Performance of Mesoscopic Soft Materials and Engineering Principles. *Chem. Soc. Rev.* **2015**, *44*, 7881−7915.

(11) Eisoldt, L.; Smith, A.; Scheibel, T. Decoding the Secrets of Spider Silk. *Mater. Today* **2011**, *14*, 80−86.

(12) Ling, S. J.; Kaplan, D. L.; Buehler, M. J. Nanofibrils in Nature and Materials Engineering. *Nat. Rev. Mater.* **2018**, *3*, 18016.

(13) Vollrath, F.; Knight, D. P. Liquid Crystalline Spinning of Spider Silk. *Nature* **2001**, *410*, 541−548.

(14) Keten, S.; Xu, Z.; Ihle, B.; Buehler, M. J. Nanoconfinement Controls Stiffness, Strength and Mechanical Toughness of β-Sheet Crystals in Silk. *Nat. Mater.* **2010**, *9*, 359−367.

(15) Giesa, T.; Arslan, M.; Pugno, N. M.; Buehler, M. J. Nanoconfinement of Spider Silk Fibrils Begets Superior Strength, Extensibility, and Toughness. *Nano Lett.* **2011**, *11*, 5038−5046.

(16) Ling, S.; Qin, Z.; Li, C.; Huang, W.; Kaplan, D. L.; Buehler, M. J. Polymorphic Regenerated Silk Fibers Assembled through Bioinspired Spinning. *Nat. Commun.* **2017**, *8*, 1387.

(17) Ling, S.; Li, C.; Jin, K.; Kaplan, D. L.; Buehler, M. J. Liquid Exfoliated Natural Silk Nanofibrils: Applications in Optical and Electrical Devices. *Adv. Mater.* **2016**, *28*, 7783−7790.

(18) Ling, S.; Jin, K.; Kaplan, D. L.; Buehler, M. J. Ultrathin Free-Standing *Bombyx Mori* Silk Nanofibril Membranes. *Nano Lett.* **2016**, *16*, 3795−3800.

(19) Chen, J.; Zhuang, A.; Shao, H.; Hu, X.; Zhang, Y. Robust Silk Fibroin/Bacterial Cellulose Nanoribbon Composite Scaffolds with Radial Lamellae and Intercalation Structure for Bone Regeneration. *J. Mater. Chem. B* **2017**, *5*, 3640−3650.

(20) Zhang, F.; You, X.; Dou, H.; Liu, Z.; Zuo, B.; Zhang, X. Facile Fabrication of Robust Silk Nanofibril Films *via* Direct Dissolution of Silk in $CaCl_2$-Formic Acid Solution. *ACS Appl. Mater. Interfaces* **2015**, *7*, 3352−3361.

(21) Nguyen, A. T.; Huang, Q. L.; Yang, Z.; Lin, N.; Xu, G.; Liu, X. Y. Crystal Networks in Silk Fibrous Materials: From Hierarchical Structure to Ultra Performance. *Small* **2015**, *11*, 1039−1054.

(22) Greving, I.; Cai, M.; Vollrath, F.; Schniepp, H. C. Shear-Induced Self-Assembly of Native Silk Proteins into Fibrils Studied by Atomic Force Microscopy. *Biomacromolecules* **2012**, *13*, 676−682.

(23) Bai, S.; Zhang, X.; Lu, Q.; Sheng, W.; Liu, L.; Dong, B.; Kaplan, D. L.; Zhu, H. Reversible Hydrogel-Solution System of Silk with High β-Sheet Content. *Biomacromolecules* **2014**, *15*, 3044−3051.

(24) Bai, S.; Zhang, W.; Lu, Q.; Ma, Q.; Kaplan, D. L.; Zhu, H. Silk Nanofiber Hydrogels with Tunable Modulus to Regulate Nerve Stem Cell Fate. *J. Mater. Chem. B* **2014**, *2*, 6590−6600.

(25) Cheng, Q.; Zhang, B.; He, Y.; Lu, Q.; Kaplan, D. L. Silk Nanofibers as Robust and Versatile Emulsifiers. *ACS Appl. Mater. Interfaces* **2017**, *9*, 35693−35700.

(26) Wang, L.; Lu, G.; Lu, Q.; Kaplan, D. L. Controlling Cell Behavior on Silk Nanofiber Hydrogels with Tunable Anisotropic Structures. *ACS Biomater. Sci. Eng.* **2018**, *4*, 933−941.

(27) Gong, Z.; Huang, L.; Yang, Y.; Chen, X.; Shao, Z. Two Distinct β-Sheet Fibrils from Silk Protein. *Chem. Commun.* **2009**, *48*, 7506−7508.

(28) Liu, Y.; Ling, S.; Wang, S.; Chen, X.; Shao, Z. Thixotropic Silk Nanofibril-Based Hydrogel with Extracellular Matrix-Like Structure. *Biomater. Sci.* **2014**, *2*, 1338−1342.

(29) Ma, M.; Zhong, J.; Li, W.; Zhou, J.; Yan, Z.; Ding, J.; He, D. Comparison of Four Synthetic Model Peptides to Understand the Role of Modular Motifs in the Self-Assembly of Silk Fibroin. *Soft Matter* **2013**, *9*, 11325−11333.

(30) Zhang, X.; Fan, Z.; Lu, Q.; Huang, Y.; Kaplan, D. L.; Zhu, H. Hierarchical Biomineralization of Calcium Carbonate Regulated by Silk Microspheres. *Acta Biomater.* **2013**, *9*, 6974−6980.

(31) Ling, S.; Li, C.; Adamcik, J.; Wang, S.; Shao, Z.; Chen, X.; Mezzenga, R. Directed Growth of Silk Nanofibrils on Graphene and Their Hybrid Nanocomposites. *ACS Macro Lett.* **2014**, *3*, 146−152.

(32) Wang, Y.; Aurelio, D.; Li, W.; Tseng, P.; Zheng, Z.; Li, M.; Kaplan, D. L.; Liscidini, M.; Omenetto, F. G. Modulation of Multiscale 3D Lattices through Conformational Control: Painting Silk Inverse Opals with Water and Light. *Adv. Mater.* **2017**, *29*, 1702769.

(33) Yu, K.; Lu, F.; Li, Q.; Chen, H.; Lu, B.; Liu, J.; Li, Z.; Dai, F.; Wu, D.; Lan, G. *In Situ* Assembly of Ag Nanoparticles (AgNPs) on

DOI: 10.1021/acsnano.8b03943
ACS Nano 2018, 12, 11860−11870

Porous Silkworm Cocoon-Based Would Film: Enhanced Antimicrobial and Wound Healing Activity. *Sci. Rep.* **2017**, *7*, 2107.
(34) Liu, W.; Zhou, Z.; Zhang, S.; Shi, Z.; Tabarini, J.; Lee, W.; Zhang, Y.; Gilbert Corder, S. N.; Li, X.; Dong, F.; Cheng, L.; Liu, M.; Kaplan, D. L.; Omenetto, F. G.; Zhang, G.; Mao, Y.; Tao, T. H. Precise Protein Photolithography (P(3)): High Performance Biopatterning Using Silk Fibroin Light Chain as the Resist. *Adv. Sci.* **2017**, *4*, 1700191.
(35) Tian, D.; Li, T.; Zhang, R.; Wu, Q.; Chen, T.; Sun, P.; Ramamoorthy, A. Conformations and Intermolecular Interactions in Cellulose/Silk Fibroin Blend Films: A Solid-State NMR Perspective. *J. Phys. Chem. B* **2017**, *121*, 6108−6116.
(36) Dong, X.; Zhao, Q.; Xiao, L.; Lu, Q.; Kaplan, D. L. Amorphous Silk Nanofiber Solutions for Fabricating Silk-Based Functional Materials. *Biomacromolecules* **2016**, *17*, 3000−3006.
(37) Wang, H. Y.; Chen, Y. Y.; Zhang, Y. Q. Processing and Characterization of Powdered Silk Micro- and Nanofibers by Ultrasonication. *Mater. Sci. Eng., C* **2015**, *48*, 444−452.
(38) Zhang, F.; Lu, Q.; Ming, J.; Dou, H.; Liu, Z.; Zuo, B.; Qin, M.; Li, F.; Kaplan, D. L.; Zhang, X. Silk Dissolution and Regeneration at the Nanofibril Scale. *J. Mater. Chem. B* **2014**, *2*, 3879−3885.
(39) Zhang, F.; Lu, Q.; Yue, X.; Zuo, B.; Qin, M.; Li, F.; Kaplan, D. L.; Zhang, X. Regeneration of High-Quality Silk Fibroin Fiber by Wet Spinning from $CaCl_2$-Formic Acid Solvent. *Acta Biomater.* **2015**, *12*, 139−145.
(40) Liu, H.; Yang, Q.; Zhang, L.; Zhuo, R.; Jiang, X. Synthesis of Carboxymethyl Chitin in Aqueous Solution and Its Thermo- and pH-Sensitive Behaviors. *Carbohydr. Polym.* **2016**, *137*, 600−607.
(41) Nie, J.; Wang, Z.; Hu, Q. Difference between Chitosan Hydrogels *via* Alkaline and Acidic Solvent Systems. *Sci. Rep.* **2016**, *6*, 36053.
(42) Luo, X. G.; Zhang, L. N. New Solvents and Functional Materials Prepared from Cellulose Solutions in Alkali/Urea Aqueous System. *Food Res. Int.* **2013**, *52*, 387−400.
(43) Duan, J.; Liang, X.; Cao, Y.; Wang, S.; Zhang, L. High Strength Chitosan Hydrogels with Biocompatibility *via* New Avenue Based on Constructing Nanofibrous Architecture. *Macromolecules* **2015**, *48*, 2706−2714.
(44) Cai, J.; Zhang, L. Rapid Dissolution of Cellulose in LiOH/Urea and NaOH/Urea Aqueous Solutions. *Macromol. Biosci.* **2005**, *5*, 539−548.
(45) Cai, J.; Zhang, L.; Zhou, J.; Qi, H.; Chen, H.; Kondo, T.; Chen, X.; Chu, B. Multifilament Fibers Based on Dissolution of Cellulose in NaOH/Urea Aqueous Solution: Structure and Properties. *Adv. Mater.* **2007**, *19*, 821−825.
(46) Cai, J.; Wang, L.; Zhang, L. Influence of Coagulation Temperature on Pore Size and Properties of Cellulose Membranes Prepared from NaOH−Urea Aqueous Solution. *Cellulose* **2007**, *14*, 205−215.
(47) Luo, X.; Zhang, L. Immobilization of Penicillin G Acylase in Epoxy-Activated Magnetic Cellulose Microspheres for Improvement of Biocatalytic Stability and Activities. *Biomacromolecules* **2010**, *11*, 2896−2903.
(48) Cai, J.; Zhang, L.; Chang, C.; Cheng, G.; Chen, X.; Chu, B. Hydrogen-Bond-Induced Inclusion Complex in Aqueous Cellulose/LiOH/Urea Solution at Low Temperature. *ChemPhysChem* **2007**, *8*, 1572−1579.
(49) Cai, J.; Zhang, L.; Liu, S.; Liu, Y.; Xu, X.; Chen, X.; Chu, B.; Guo, X.; Xu, J.; Cheng, H.; Han, C. C.; Kuga, S. Dynamic Self-Assembly Induced Rapid Dissolution of Cellulose at Low Temperatures. *Macromolecules* **2008**, *41*, 9345−9351.
(50) Zhou, J. P.; Zhang, L. N. Solubility of Cellulose in NaOH/Urea Aqueous Solution. *Polym. J.* **2000**, *32*, 866−870.
(51) Deyoung, L. R.; Dill, K. A.; Fink, A. L. Aggregation and Denaturation of Apomyoglobin in Aqueous Urea Solutions. *Biochemistry* **1993**, *32*, 3877−3886.
(52) Bian, L. J.; Yang, X. Y. Effect of Denaturant Concentration on Hen-Egg White Lysozyme Renaturation. *Chin. J. Chem.* **2006**, *24*, 653−659.
(53) Peng, Q.; Zhang, Y.; Lu, L.; Shao, H.; Qin, K.; Hu, X.; Xia, X. Recombinant Spider Silk from Aqueous Solutions *via* a Bio-Inspired Microfluidic Chip. *Sci. Rep.* **2016**, *6*, 36473.
(54) Deng, Y.; Zhang, G.; Yi, S.; Hu, Y.; Wang, Y.; Qin, F. Influence of Urea on the Raw Silk Degum Using Papain. *Text. Res. J.* **2013**, *34*, 81−84.
(55) Lin, L. N.; Brandts, J. F. Further Evidence Suggesting That the Slow Phase in Protein Unfolding and Refolding Is Due to Proline Isomerization: A Kinetic Study of Carp Parvalbumins. *Biochemistry* **1978**, *17*, 4102−4110.
(56) Berghausen, J.; Zipfel, J.; Lindner, P.; Richtering, W. Influence of Water-Soluble Polymers on the Shear-Induced Structure Formation in Lyotropic Lamellar Phases. *J. Phys. Chem. B* **2001**, *105*, 11081−11088.
(57) Marsh, R. E.; Corey, R. B.; Pauling, L. An Investigation of the Structure of Silk Fibroin. *Biochim. Biophys. Acta* **1955**, *16*, 1−34.
(58) Koh, L. D.; Cheng, Y.; Teng, C. P.; Khin, Y. W.; Loh, X. J.; Tee, S. Y.; Low, M.; Ye, E. Y.; Yu, H. D.; Zhang, Y. W.; Han, M. Y. Structures, Mechanical Properties and Applications of Silk Fibroin Materials. *Prog. Polym. Sci.* **2015**, *46*, 86−110.
(59) Gosline, J. M.; Demont, M. E.; Denny, M. W. The Structure and Properties of Spider Silk. *Endeavour* **1986**, *10*, 37−43.
(60) Termonia, Y. Molecular Modeluing of Spider Silk Elasticity. *Macromolecules* **1994**, *27*, 7378−7381.
(61) Vollrath, F.; Holtet, T.; Thogersen, H. C.; Frische, S. Structural Organization of Spider Silk. *Proc. R. Soc. London, Ser. B* **1996**, *263*, 147−151.
(62) Vollrath, F.; Porter, D. Spider Silk as Archetypal Protein Elastomer. *Soft Matter* **2006**, *2*, 377−385.
(63) Porter, D.; Vollrath, F. Silk as a Biomimetic Ideal for Structural Polymers. *Adv. Mater.* **2009**, *21*, 487−492.
(64) Lin, Z.; Huang, W.; Zhang, J.; Fan, J. S.; Yang, D. Solution Structure of Eggcase Silk Protein and Its Implications for Silk Fiber Formation. *Proc. Natl. Acad. Sci. U. S. A.* **2009**, *106*, 8906−8911.
(65) Jin, H. J.; Kaplan, D. L. Mechanism of Silk Processing in Insects and Spiders. *Nature* **2003**, *424*, 1057−1061.
(66) Hagn, F.; Eisoldt, L.; Hardy, J. G.; Vendrely, C.; Coles, M.; Scheibel, T.; Kessler, H. A Conserved Spider Silk Domain Acts as a Molecular Switch That Controls Fibre Assembly. *Nature* **2010**, *465*, 239−242.
(67) Vollrath, F.; Porter, D. Spider Silk as a Model Biomaterial. *Appl. Phys. A: Mater. Sci. Process.* **2006**, *82*, 205−212.
(68) Wu, X.; Liu, X.-Y.; Du, N.; Xu, G.; Li, B. Unraveled Mechanism in Silk Engineering: Fast Reeling Induced Silk Toughening. *Appl. Phys. Lett.* **2009**, *95*, 093703.
(69) Pan, H.; Zhang, Y.; Shao, H.; Hu, X.; Li, X.; Tian, F.; Wang, J. Nanoconfined Crystallites Toughen Artificial Silk. *J. Mater. Chem. B* **2014**, *2*, 1408−1414.
(70) Allaire, M.; Yang, L. Biomolecular Solution X-Ray Scattering at the National Synchrotron Light Source. *J. Synchrotron Radiat.* **2011**, *18*, 41−44.
(71) Essmann, U.; Perera, L.; Berkowitz, M. L.; Darden, T.; Lee, H.; Pedersen, L. G. A Smooth Particle Mesh Ewald Method. *J. Chem. Phys.* **1995**, *103*, 8577−8593.
(72) Hess, B.; Bekker, H.; Berendsen, H. J. C.; Fraaije, J. G. E. M. Lincs: A Linear Constraint Solver for Molecular Simulations. *J. Comput. Chem.* **1997**, *18*, 1463−1472.
(73) Hess, B.; Kutzner, C.; van der Spoel, D.; Lindahl, E. GROMACS 4: Algorithms for Highly Efficient, Load-Balanced, and Scalable Molecular Simulation. *J. Chem. Theory Comput.* **2008**, *4*, 435−447.
(74) Best, R. B.; Zhu, X.; Shim, J.; Lopes, P. E. M.; Mittal, J.; Feig, M.; MacKerell, A. D. Optimization of the Additive Charmm All-Atom Protein Force Field Targeting Improved Sampling of the Backbone Φ, Ψ and Side-Chain X(1) and X(2) Dihedral Angles. *J. Chem. Theory Comput.* **2012**, *8*, 3257−3273.

DOI: 10.1021/acsnano.8b03943
ACS Nano 2018, 12, 11860−11870